Primary Frequency Control in Isolated Microgrids using Thermostatically Controllable Loads

William Mendieta, and Claudio A. Cañizares, *Fellow, IEEE*

***Abstract*—Hybrid renewable energy sources (RES)-diesel systems are now being considered as an economic, attractive and clean option for remote isolated microgrids, to offset diesel consumption by displacing generation from conventional units; however, system security and stability is a challenge as the penetration of RES increases. In this context, Demand Response (DR) can be used to increase grid flexibility, improve efficiency, and facilitate the penetration of RES. Thermostatically controllable loads (TCLs), i.e., electric water heaters (EWHs), air conditioners (ACs), and ground source heat pumps (GSHPs), are ideal candidates to participate in such a DR strategy, since their power consumption can be controlled without affecting consumer comfort. Therefore, this paper presents novel, computationally efficient, and adequate thermo-electrical dynamic models of ACs and GSHPs, along with an existing model of EWHs, to adapt and improve a decentralized DR strategy for Direct Load Control (DLC) for primary frequency regulation in hybrid isolated microgrids. Different cases studies are presented for a real microgrid to analyze and compare the system frequency response and determine the adequacy of the proposed approach and models, demonstrating their effectiveness for primary frequency control provision to facilitate higher RES penetrations.**

***Index Terms*—Air conditioner, demand response, electric water heater, ground source heat pump, hybrid isolated microgrid, primary frequency control.**

NOMENCLATURE

A. Parameters

ΔT	Half dead band temperature [°C]
η_{WH}	Efficiency of the EWH [%]
ρ_w	Density of water [kg/m^3]
τ_D	Engine firing time delay [s]
τ_i	Time constants of the DEGOV$_1$ governor model
ω_{ref}	Reference speed [p.u.]
A_1-F_1	Equation fit coefficients
C_i	Thermal capacitance of the indoor air [J/°C]
C_m	Thermal capacitance of the concrete slab foundation [°C/W]
C_{wt}	Thermal capacitance of water [J/°C]
EER_{ref}	Rated energy efficiency ratio of the HP
$f_{min/max}$	Min./max. frequency limits [Hz]
f_0	Target frequency [Hz]
k_f	Temperature-frequency coefficient [°C/Hz]
$P_{AC,ref}$	Rated power of the AC [W]
P_{WH}	Rated power of the EWH [W]
$Q_{AC,ref}$	Rated cooling capacity of the AC [W]
$Q_{c,ref}$	Rated cooling capacity of the HP [W]
Q_{in}	Internal heat gains [W]
Q_s	Solar irradiation on external walls [W]
R_c	Thermal resistance of the external glazed surfaces [°C/W]
R_m	Thermal resistance of the concrete slab foundation [°C/W]
R_w	Half thermal resistance of the building envelope (walls+ceiling) [°C/W]
T_{amb}	Outdoor temperature [°C]
T_{base}	Target temperature [°C]
$T_{i,min}$	Indoor temperature lower limit [°C]
$T_{i,max}$	Indoor temperature upper limit [°C]
T_{in}	Inlet cold water temperature [°C]
T_{MAX}	Upper torque limit [p.u.]
T_{MIN}	Lower torque limit [p.u.]
T_{ref}	Reference temperature (283 °K)
Tw_{in}	Inlet fluid temperature [°C]
$T_{WH,min}$	Hot water temperature lower limit [°C]
$T_{WH,max}$	Hot water temperature upper limit [°C]
UA	Thermal conductance of the tank shell [W/°C]
V_{air}	Indoor air volumetric flow rate [m^3/s]
$V_{air,ref}$	Indoor air volumetric flow rate reference [m^3/s]
V_T	Genset output voltage [V]
W_d	Average hot water drawn per hour [gal/h]
X_1-Y_4	Equation fit coefficients
c_{pw}	Specific heat capacity of water [J/kg ·°C]
s_p	Slope factor [kW/Hz]
$\dot{m}_W$	Mass flow rate of fluid through the GHX [kg/h]
$\dot{m}_{W,ref}$	Mass flow rate reference [kg/h]

B. Variables

EER	Energy efficiency ratio - AC/GSHP
f_{sys}	System frequency [Hz]
P_{AC}	Power consumed by the compressor [W]
P_G	Active power supplied to the system [W]
Q_{AC}	Heat absorbed by the AC system [W]
Q_c	Cooling capacity of the HP [W]
Q_{GS}	Heat injected/absorbed by the GSHP system [W]
Q_{WH}	Heat injected into the tank [W]
s(t)	Thermostat switch position
$T_{db,ODC}$	Outdoor dry-bulb temperature [°C]
T_i	Indoor temperature [°C]
T_m	Temperature of the concrete slab foundation [°C]
T_w	Temperature on external walls [°C]
T_{db}	Indoor dry-bulb temperature [°C]
T_{wb}	Indoor wet-bulb temperature [°C]

This work has been supported by the Secretariat of Higher Education, Science, Technology and Innovation (SENESCYT) of Ecuador, and the Natural Sciences and Engineering Research Council's (NSERC) Energy Storage Technology Network (NESTNet) of Canada.

The authors are with the Department of Electrical and Computer Engineering, University of Waterloo, Waterloo, ON N2L 3G1, Canada (e-mail: wmendiet@uwaterloo.ca; ccanizar@uwaterloo.ca).

$T_{wb,IDC}$	Indoor wet-bulb temperature [°C]
T_{WH}	Temperature of the water inside the tank [°C]
Tw_{out}	HP outlet fluid temperature [°C]
Tw_{in}	HP inlet fluid temperature [°C]
T_0	Thermostat setpoint temperature [°C]
$\dot{m}_{WH}$	Inlet water mass flow rate [kg/h]

I. Introduction

To ameliorate the known economic and environmental issues with diesel-based microgrids, especially in remote microgrids [1]–[3], hybrid systems can be used as a cost-effective alternative that combine conventional diesel generation with Renewable Energy Sources (RES). This energy supply mix provides a cleaner choice to increase energy security, reduce diesel consumption, and lower electricity prices [1]. However, maintaining the demand-supply balance in a hybrid microgrid is challenging because of the variable nature of RES. As a result, the system operates under continuous power imbalances, which if not compensated for, may lead to large frequency deviations [4]. Consequently, among the major challenges of integrating RES, is a need for frequency control mechanisms with higher flexibility based on energy storage technologies to counter the stress caused by RES, instead of forcing costly diesel gensets to respond quickly to maintain frequency stability.

One possibility for relieving the variability of RES and providing frequency reserves is making strategic power demand adjustments, which is known as Demand Response (DR). By using Thermostatically Controllable Loads (TCLs), through a DR strategy, many grid support services can be provided [5]. These types of loads, i.e., Electric Water Heaters (EWHs), Air Conditioners (ACs), Ground Source Heat Pumps (GSHPs), Electric Space Heaters (ESHs), refrigerators, and freezers, while providing thermal services, have thermal inertias that allow instantaneous decoupling of the thermal load from their electricity consumption without compromising end-users' comfort. EWHs and refrigerators are the most common types of TCLs available in houses worldwide. The typical arrangement for a residential Heat, Ventilation, and Air Conditioning (HVAC) system consists of a central forced-air system along with an AC and a furnace [6]. However, according to [7], a GSHP is the most environment-friendly, efficient, and clean alternative for space climate conditioning that can be used almost any place, significantly reducing power consumption by using geothermal energy as a source/sink of heat for climate control.

DR aims to control TCL switching actions in response to system frequency deviations [8]–[12]. For example, in [8], primary frequency control is provided in a hybrid isolated microgrid using EWHs. However, some simplified assumptions are used, such as that all households have similar hourly averaged load and hot water usage profiles, irrespective of the number of occupants, which, as explained in [9], is not realistic. In [10], it is shown that a population of refrigerators can provide aggregated frequency reserves in an amount equivalent to their total average power consumption. Moreover, in [11], a DR strategy is presented for improving frequency stability by using refrigerators and freezers that are turned ON/OFF to maintain system frequency within a specified band, so that, when the frequency varies, the demand is dynamically adjusted. However, due to their low rated power, the aggregated frequency reserve might be insufficient to counter large frequency deviations in an isolated microgrid. In [12], two methods are presented to correct frequency deviations by measuring frequency locally. The first method defines a frequency dead band located below the nominal system frequency. If the frequency goes below the lower limit, TCLs are turned OFF until the frequency recovers and surpasses the upper limit. The second method uses a linear temperature-frequency relationship (the same principle used in [8]), continuously adjusting the demand as a function of frequency deviations. Both methods have been applied to EWHs and ESHs in a large power system with promising results. The control logic from these methods can be modified and adapted for other types of TCLs such as ACs and GSHPs for the provision of primary frequency control in an isolated microgrid, as demonstrated here.

Mathematical models have been developed to reproduce the thermo-electrical behavior of TCLs [13]. However, it is necessary to identify a proper model and consider a speed-accuracy trade-off when a TCL provides frequency control. Therefore, the thermal model choice must be computationally efficient, simple, and accurate enough to capture the required dynamics over the simulation time-horizon [14]. In the specific case of ACs and GSHPs, fast dynamic simulations are highly complex due to the difficulty of linking the responses of their components to obtain a complete thermo-electrical picture of their behavior [15].

Based on the discussions above and [16], the following are the main objectives and contributions of this paper:

- Develop models of residential TCLs, i.e., ACs, and GSHPs, to properly reproduce their thermo-electrical response for DR dynamic applications.
- Develop a frequency-based DR strategy for TCLs to provide primary frequency control.
- Evaluate, demonstrate, and validate the practical effectiveness of the proposed DR strategy in a real isolated microgrid with high RES penetration.

The rest of the paper is organized as follows: Section II presents the main background required to develop the proposed DR strategy, followed by a review of the components, operation, and restrictions of TCLs. Section III describes the modeling of the TCLs and discusses the design of the DR strategy for primary frequency control. In Section IV, several case studies are performed to analyze and compare the frequency response of a real isolated microgrid with TCLs for different controls, and relevant results are presented and discussed. Finally, the main conclusions are presented in Section V.

II. BACKGROUND

A. Demand Response

Based on the available resources, i.e., communication channels and type of controllable loads, and the control strategy

adopted, DR may provide various frequency support services on different time scales (e.g., regulation, ramping, spinning reserves) [12]. In fact, DR may present frequency regulation performance characteristics that are not available from various conventional regulation providers, based on load elasticity in time-scales ranging from fractions of seconds to minutes, or even hours [9]. Since TCLs are fast-acting resources, DR control of such a cluster of loads may provide primary frequency regulation services, as discussed in [8]. In this context, DR primary frequency regulation with TCLs may be based on ON/OFF load operation as a function of frequency deviations to help resolve generator-load power imbalances, as discussed next.

B. AC

An split AC system consists of four main components: compressor, condenser, expansion valve, and evaporator [17]. ACs' switching actions are restricted by a lockout time after being turned OFF to avoid compressor stall. Consequently, a DR strategy has to consider this lockout time when controlling the duty cycle of the AC to provide frequency control.

C. GSHP

This system uses the ground as a heat sink in summer and as a heat source in winter. Thus, the GSHP pumps heat to the ground so as to cool the household; otherwise, the GSHP absorbs heat from the ground and releases it into the household. According to [18], the system most commonly used in North America has a vertical ground heat exchanger (GHX), because of the minor land area required to drill the boreholes; therefore, only this type of system is considered here. A GSHP with a vertical GHX consists of a compact water-to-air heat pump (HP) which is connected to an external closed loop circuit and an internal open loop circuit. The external circuit includes one or more boreholes drilled into the ground where heat is exchanged between the borehole and its surrounding ground. On the other hand, the internal circuit comprises the forced-air distribution system inside the household. When a GSHP is working in cooling mode, it performs a refrigeration-cycle. Otherwise, the refrigerant flow is reversed, and both HXs switch their functions; thus, the GSHP performs a heat-pump-cycle. For the cooling mode, the coefficient of performance is known as the EER (analog to that of an AC), whereas for the heating mode it is simply COP. In addition, GSHPs have the same restriction as conventional ACs, requiring a lockout time when it is turned OFF to avoid compressor stall.

D. EWH

A residential EWH has an insulated metal-sheet cylindrical tank where hot water is stored until it is needed. The tank includes one or two heating elements, an inlet pipe for the cold water, and an outlet pipe for the hot water. Each heating element has a thermostat, which is attached to an electrical resistor enclosed by a sheath of stainless steel or copper. Since the heating element contains a resistor, its power consumption can be controlled as fast and frequently as needed to provide frequency control.

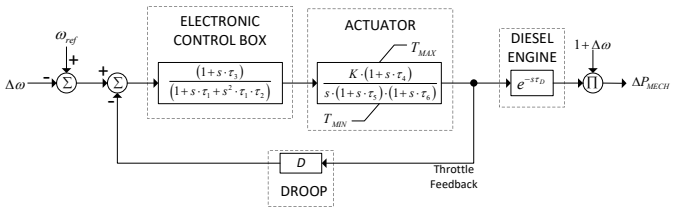


Fig. 1. Block diagram of the diesel genset DEGOV_1 governor model [19].

TABLE I
PARAMETERS OF THE DEGOV_1 GOVERNOR MODEL [20].

Parameter	Value
τ_1 [s]	0.01
τ_2 [s]	0.02
τ_3 [s]	0.2
τ_4 [s]	0.25
τ_5 [s]	0.009
τ_6 [s]	0.0384
T_{MIN} [p.u.]	0
T_{MAX} [p.u.]	1.1
τ_D [s]	0.01

III. MODELING AND CONTROLS

The Thermal Equivalent Circuit (TEC) method is adopted to model the thermodynamic processes. This method represents heat transfer processes by means of an electrical circuit. Then, based on circuit solution techniques, the differential equations that describe the thermodynamic processes are formulated.

A. Diesel Gensets

The standard Woodward governor model DEGOV_1 is used here [19], which consists of three components: an electronic control box, a fuel control actuator, and a droop compensator; Fig. 1 presents a block diagram of the DEGOV_1 model used. The gains and time constants used in this model are adopted from [20] and are summarized in Table I.

B. EWH

Fig. 2 depicts the TEC model of the EWH under study, from which the following ordinary differential equation describing the heat transfer processes can be obtained:

$$C_{wt}\frac{dT_{WH}}{dt} = \dot{m}_{WH}\, c_{pw}\,(T_{in} - T_{WH}) + UA\,(T_i - T_{WH}) + s_{WH}(t)\, Q_{WH} \tag{1}$$

where:

$$\dot{m}_{WH} = W_d(t)\,\rho_w \tag{2}$$

$$Q_{WH} = P_{WH}\,\eta_{WH} \tag{3}$$

Fig. 3 shows the thermo-electrical response of an EWH for a family of five occupants, using the parameters of the EWH summarized in Table II. The plots are based on the 24-h hot water usage profile obtained from the DHW Event Schedule Generator [21], for a 50 gallons capacity. The EWH is controlled by a thermostat which setpoint is 50 °C and has

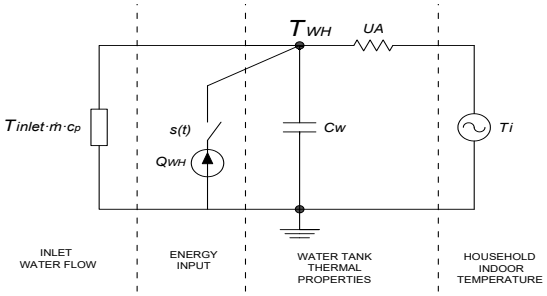


Fig. 2. TEC network of a single-element tank-type EWH [6].

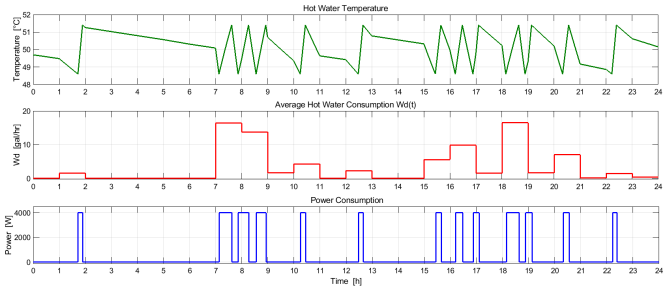


Fig. 3. Results of the EWH modeling.

TABLE II
CHARACTERISTICS OF THE EWH [6]

Parameter	Value
ρ_w [kg/m^3]	998
c_{pw} [J/kg·°C]	4180
T_{in} [°C]	16
UA [W/°C]	6847.483
P_{WH} [W]	4000
η_{WH} [%]	94

a $\pm$ 1.4 °C dead band. The power consumed by the EWH depends on T_{WH}; thus, as soon as this temperature hits the lower dead band limit, the heating element of the EWH is turned ON, remaing in this state until T_{WH} hits the upper dead band limit.

C. AC

The model of an AC system consists of three components: (1) TEC model of a household, (2) equation fit model of the AC, and (3) outdoor temperature profile, as depicted in Fig. 4.

1) Household: The TEC model depicted in Fig. 5 is used to study the thermodynamic response of the household, which yields the following set of differential equations describing the heat transfer processes:

$$C_m \frac{dT_m}{dt} = \frac{1}{R_m}\left(T_i - T_m\right) \tag{4}$$

$$C_w \frac{dT_w}{dt} = Q_s + \frac{1}{R_w}\left(T_{amb} - T_w\right) + \frac{1}{R_w}\left(T_i - T_w\right) \tag{5}$$

$$C_i \frac{dT_i}{dt} = Q_{in} \pm s(t)\, Q_{AC/GS} + \frac{1}{R_w}\left(T_w - T_i\right) + \frac{1}{R_c}\left(T_{amb} - T_i\right) - \frac{1}{R_m}\left(T_m - T_i\right) \tag{6}$$

2) AC: The equation fit model presented in [22] is adopted here, in which the equation fit coefficients are determined by a least-square fit of a manufacturer's catalogue data. Thus, the correlations used to model the AC are formulated as follows:

$$\frac{Q_{AC}}{Q_{AC,ref}} = X_1 + X_2\left[\frac{T_{db,ODC}}{T_{ref}}\right] + X_3\left[\frac{T_{wb,IDC}}{T_{ref}}\right] + X_4\left[\frac{\dot{V}_{air}}{\dot{V}_{air,ref}}\right] \tag{7}$$

$$\frac{P_{AC}}{P_{AC,ref}} = Y_1 + Y_2\left[\frac{T_{db,ODC}}{T_{ref}}\right] + Y_3\left[\frac{T_{wb,IDC}}{T_{ref}}\right] + Y_4\left[\frac{\dot{V}_{air}}{\dot{V}_{air,ref}}\right] \tag{8}$$

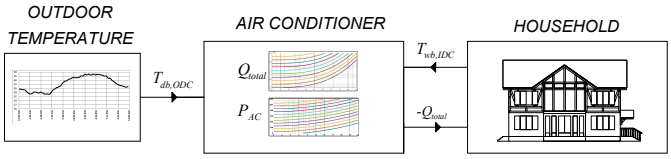


Fig. 4. Correlations between the sub-models of an AC.

where Q_{AC} is used as input to the TEC model of the household, and $T_{wb,IDC}$ is computed as function of both the dry-bulb temperature $T_{db,IDC}$ and the relative humidity, as per [23].

3) Household+AC model: Fig. 6 shows the relationships between the inputs (red), internal processes (black), and output (green) used to model the household thermal behavior and AC power consumption. At each time step, the model uses the inputs and simultaneously solves the household and AC sub-models until it converges.

An AC is selected among the manufacturers' catalogue with similar cooling capacity than the GSHP, in order to compare their cycling and power consumptions under the same conditions. The characteristics of the AC are shown in Table III. The AC is controlled by a thermostat with a 25 °Csetpoint, and a $\pm$ 0.5 °C dead band. Fig. 7 shows the thermo-electrical response of the household+AC model. Note that the pattern of the power consumption changes dynamically as the cooling load changes.

D. GSHP

The model of a GSHP consists of: (1) TEC model of the household, (2) equation fit model of the reversible water-to-air HP, and (3) TEC model of the GHX, as depicted in Fig. 8. The model of the household is the same developed for the AC.

1) HP: Similarly to the AC, an equation fit model is used to model the thermo-electrical response of the HP. The cooling mode equations are formulated as follows [25]:

$$\frac{Q_c}{Q_{c,ref}} = A_1 + B_1\left[\frac{T_{Win}}{T_{ref}}\right] + C_1\left[\frac{T_{ref}}{T_{wb}}\right]\left[\frac{\dot{m}_W}{\dot{m}_{W,ref}}\right] \tag{9}$$

$$\frac{EER}{EER_{ref}} = D_1 + E_1\left[\frac{T_{Win}}{T_{ref}}\right] + F_1\left[\frac{T_{ref}}{T_{db}}\right]\left[\frac{\dot{m}_W}{\dot{m}_{W,ref}}\right] \tag{10}$$

The power consumed by the compressor P_c is:

$$P_c = \frac{Q_c}{EER} \tag{11}$$

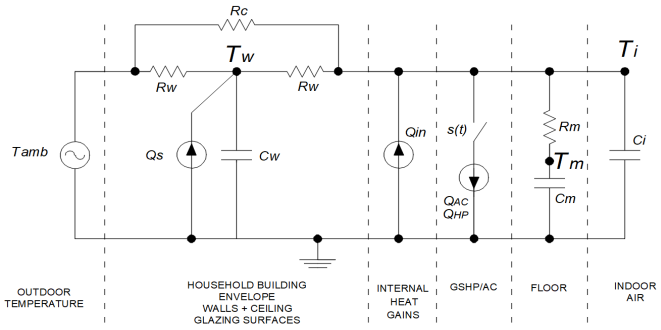


Fig. 5. TEC network model of a household.

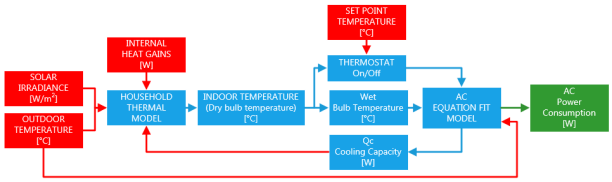


Fig. 6. Process flowchart of the household+AC model.

And the amount of heat rejected to the ground is:

$$Q_{rejected} = Q_c + P_c \tag{12}$$

Finally, Tw_{out} which is used as input to the borehole model, is computed as follows:

$$Tw_{out} = \frac{Q_{rejected}}{\dot{m}_W c_{pw}} + Tw_{in} \tag{13}$$

2) Borehole: The TEC model developed in [26] captures the short-term dynamics of the heat exchange between the borehole and its surrounding ground. A vertical discretization is used to represent the borehole by means of n segments with height dz. Then, for each segment, a TEC network is built to describe the heat transfer processes along the borehole depth, as depicted in Fig. 9. Each node represents a specific temperature, with T_1 and T_2 representing the fluid inside each leg of the U-pipe, T_{b1} and T_{b2} corresponding to the grout regions, and T_g representing the ground. To solve the heat-flow equations, the Lax-Wendroff approximation method is used. Thus, the temperature of each point j can be computed as follows:

$$T_1^{n+1}(j) = T_1^n(j) - \frac{v\Delta t}{2\Delta z}[(T_1^n(j+1) - T_1^n(j-1)) - \frac{v\Delta t}{\Delta z}(T_1^n(j+1) - 2T_1^n(j) + T_1^n(j-1))] - \frac{\Delta t}{C_f}\left(\frac{T_1^n(j) - T_{b1}^n(j)}{R_{b1}} + \frac{T_1^n(j) - T_2^n(j)}{R_{pp}}\right) \tag{14}$$

$$T_2^{n+1}(j) = T_2^n(j) - \frac{v\Delta t}{2\Delta z}[(T_2^n(j+1) - T_2^n(j-1)) - \frac{v\Delta t}{\Delta z}(T_2^n(j+1) - 2T_2^n(j) + T_2^n(j-1))] - \frac{\Delta t}{C_f}\left(\frac{T_2^n(j) - T_{b2}^n(j)}{R_{b2}} - \frac{T_1^n(j) - T_2^n(j)}{R_{pp}}\right) \tag{15}$$

TABLE III
CHARACTERISTICS OF THE TRANE 1.5 TONS AC [24]

Model	2TTB3024A1
Parameter	**Value**
Total Capacity [BTUh]	20800
Power [W]	1930

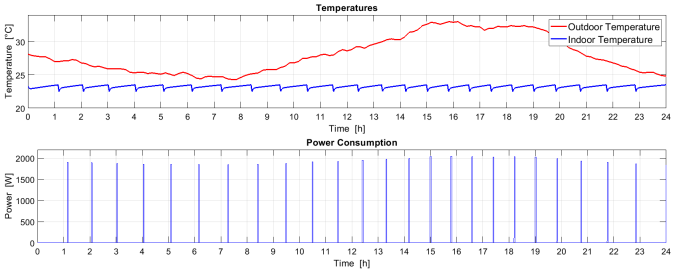


Fig. 7. Results of the household+AC modeling.

$$T_{b1}^{n+1}(j) = T_{b1}^n(j) - \frac{\Delta t}{C_{b1}}\left(\frac{T_1^n(j) - T_{b1}^n(j)}{R_{b1}} + \frac{T_{b1}^n(j) - T_{b2}^n(j)}{R_{bb}} - \frac{T_{b1}^n(j) - T_g^n(j)}{R_g}\right) \tag{16}$$

$$T_{b2}^{n+1}(j) = T_{b2}^n(j) - \frac{\Delta t}{C_{b2}}\left(\frac{T_2^n(j) - T_{b2}^n(j)}{R_{b2}} - \frac{T_{b1}^n(j) - T_{b2}^n(j)}{R_{bb}} - \frac{T_{b2}^n(j) - T_g^n(j)}{R_g}\right) \tag{17}$$

$$T_g^{n+1}(j) = T_g^n(j) + \frac{\Delta t}{C_g}\left(\frac{T_{b1}^n(j) - T_g^n(j)}{R_g} + \frac{T_{b2}^n(j) - T_g^n(j)}{R_g}\right) \tag{18}$$

The temperature of the segment $j = N$ corresponds to the temperature of the fluid leaving the GHX. This temperature is used as input to the HP model.

3) Household+GSHP model: Fig. 10 shows a schematic of the relationships between the inputs (red), internal processes (black), and output (green) used to model the thermal behavior and power consumption of the household and GSHP.

The characteristics of a GSHP are depicted in Table IV. The GSHP is controlled by a thermostat with a setpoint of 25 °C and a ± 0.5 °C dead band. The GHX has the geometric and thermal characteristics presented in [26]. Fig. 11 shows the thermo-electrical response of the household+GSHP model. The compressor cycles are reflected in the temperatures of the fluid Tw_{in} and Tw_{out} for the GHX, and the internal household air temperature T_i. Tw_{out} is lower than Tw_{in}, since as the fluid flows through the GHX, heat is transferred to the ground, and therefore, the fluid temperature decreases.

E. Primary Frequency Control Strategy

Since frequency is a global parameter that can be observed at any point in a microgrid, providing information to determine the instantaneous demand-supply balance, a DR strategy for TCLs using a decentralized control architecture is proposed here. A communication channel for frequency

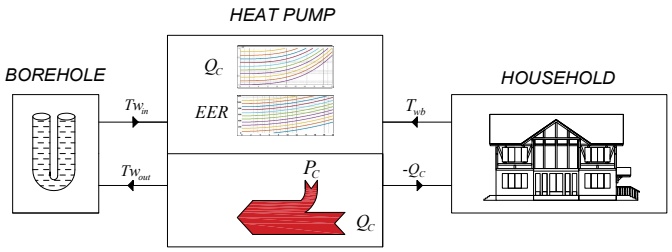


Fig. 8. Correlations between the sub-models of a GSHP.

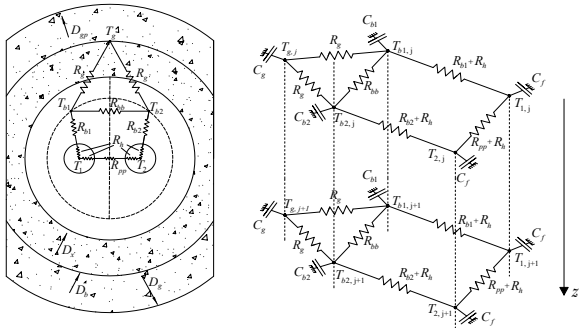


Fig. 9. TEC network model of the GHX [26].

regulation signals is unnecessary in this case, since each TCL controller should be able to measure the system frequency locally. Therefore, by means of a local frequency sensor, which is not considered in the models without loss of generality, and an adequate control logic, TCLs can be autonomously turned ON/OFF while considering consumer comfort [12], [13]. In [12] and [28], it is shown that this architecture provides a faster and smoother frequency response, since the logic decisions are taken in parallel between all controllable loads. Moreover, in [9], demand is found to react to frequency deviations in a similar way to that of conventional generators, even when there is not a two-way communication channel. In fact, conventional generators also use this type of architecture for primary frequency control, since their response is determined by a droop characteristic that uses a local frequency measurement as input [11].

Thus, the thermostat temperature setpoint T_0 is dynamically adjusted according to the system frequency deviation as follows [12]:

$$T_0 = T_{base} \pm k_f \left(f_{sys} - f_0\right) \tag{19}$$

In the case of EWHs, the parameters of (19) are determined as follows:

$$T_{base} = \frac{T_{WH,min} + T_{WH,max}}{2} \tag{20}$$

$$f_0 = \frac{f_{min} + f_{max}}{2} \tag{21}$$

$$k_f = \frac{T_{WH,max} - T_{WH,min}}{f_{max} - f_{min}} \tag{22}$$

The temperature-frequency characteristic must be complemented by a control logic in order to limit the switching operations. At each time step, the control measures f_{sys}, T_{EWH}, and $s(t)$, and also uses the previous value of the

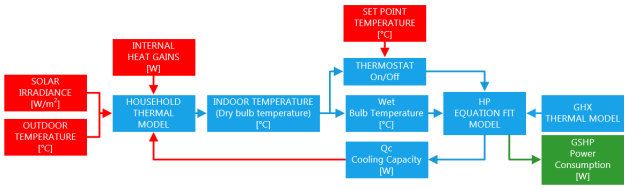


Fig. 10. Process flowchart of the household+GSHP model.

TABLE IV
CHARACTERISTICS OF BOSCH 1.5 TONS GSHP [27]

Model	BP018
Parameter	**Value**
Cooling Capacity [BTUh]	20500
EER	19

thermostat setpoint $T_{0,prev}$. If f_{sys} varies with respect to f_0, the control will increase/decrease the thermostat setpoint temperature by a factor $\Delta T_0 = k_f(f_{sys} - f_0)$. The following control logic is modified from [8] for a better performance when EWHs are providing primary frequency control:

- If $\Delta T_0 < 2\Delta T$ the control is activated.
- If $-2\Delta T < \Delta T_0$ the control is activated.
- If $\Delta T_0 > 2\Delta T$:
  - If $T_{WH} < T_{0,prev}$ and $s_{WH}(t) = 0$ the control is activated.
  - If $s_{WH}(t) = 1$ the control is activated.
- If $\Delta T_0 < -2\Delta T$:
  - If $T_{WH} > T_{0,prev}$ and $s_{WH}(t) = 1$ the control is activated.
  - If $s_{WH}(t) = 0$ the control is activated.
- Two intermediate limits (f_{low} and f_{up}) within and close to the system frequency limits are defined as follows:

$$f_{min} < f_{low} < f_0 \tag{23}$$

$$f_0 < f_{up} < f_{max} \tag{24}$$

  If $f_{sys} < f_{low}$ or $f_{sys} > f_{up}$ the control is activated.
- If $f_{sys} \leq f_{min}$ or $f_{sys} \geq f_{max}$, the slope k_f is increased.
- If $T_0 > T_{EWH,max}$ or $T_0 < T_{EWH,min}$ the control is deactivated.
- If the logic leads to disable the control, the thermostat setpoint temperature will be equal to that of the previous time step, i.e., $T_0 = T_{0,prev}$.

In the case of ACs and GSHPs, the control logic is the same than that for EWHs, but is complemented by the lockout time $t_{lockout}$ when the AC/GSHP is turned OFF. Thus, a flag t_f is used to determine if the time these TCLs have remained OFF is greater than the lockout time. The flowchart of the DLC control logic for EWHs and ACs/GSHPs are provided in Figs. 12 and 13, respectively; the proposed modifications to improve performance of the EWH control logic presented in [8] are highlighted in yellow.

The frequency control model used to study the performance of the DR strategy for the provision of primary frequency control is shown in Fig. 17, consisting of aggregated non-TCL load demand, aggregated solar PV generation, aggregated

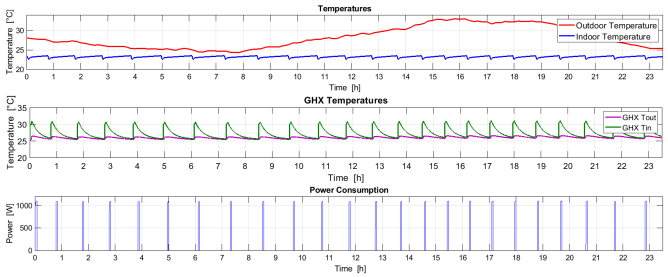


Fig. 11. Results of the household+GSHP modeling.

TCLs with DLC controllers, and aggregated Distributed Energy Sources or DERs (typically diesel gensets in practice) with governor and inertia. The controllers of the EWHs and ACs/GSHPs monitor the system frequency, and turn ON/OFF these TCLs according to the control logic described above. As shown in Figs. 12 and 13, the DR logics only uses the current thermostat status to control the TCLs, and given that their response is nearly instantaneous, the logic processes are conducted continuously to perform real-time primary frequency control.

It is important to highlight the fact that, in microgrids, voltage and frequency, i.e., active and reactive power, are coupled due to the large R/X ratio of distribution feeders, and especially the voltage dependence of loads [29]. However, in this paper, the voltage is not considered nor modeled, and only active power and associated frequency phenomena are considered, through the modeling of DER inertia and governors, and the load power demand associated with the TLC thermal response, which is the focus of the paper.

IV. MODELING VALIDATION

A. EWH

The physically-based single-element EWH depicted in Fig. 2 and adopted from [6] is used due to its simplicity to accurately reproduce the EWH's thermo-electrical behavior under the dynamic conditions associated with the proposed ON/OFF frequency control approach, as demonstrated in [8], [30]–[32].

B. AC

1) Household: The household TEC sub-model depicted in Fig. 5 is an improved version of the one presented in [6], which has been validated with actual measurements, by adding the differential equation (4), which corresponds to the heat transfer of the conditioned space through its floor, as suggested in [33] and [34]. Thus, to validate the proposed TEC model, it is assumed that the space is conditioned by an ideal AC of constant 1930 W power, which is the size of the units considered in the simulation section, when the household is exposed to the outdoor temperature curve of Fig. 7. Fig 14 shows the 12-hour simulation results obtained with both the model from [6] and the proposed TEC model, thus validating the household model (the total energy error is 0.69 %).

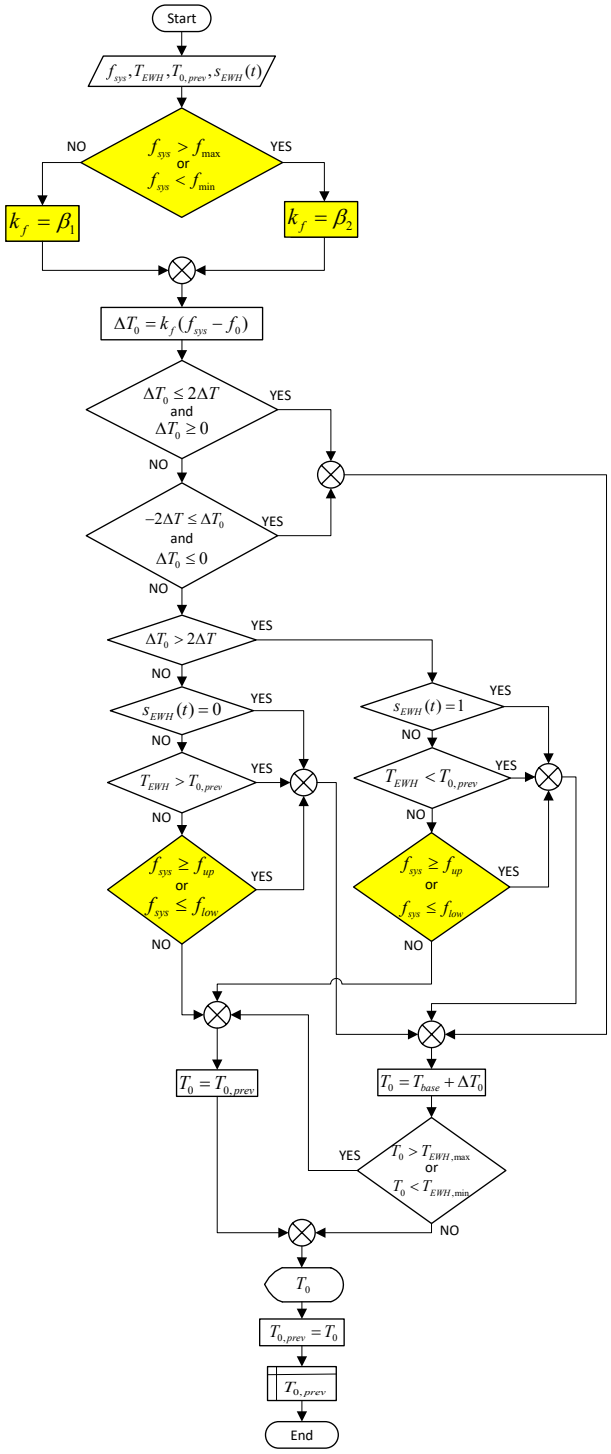


Fig. 12. Proposed DLC logic for EWHs.

2) AC: The AC sub-model given by equations (7) and (8) and adopted from [22], with 8 fit coefficients obtained from the AC manufacturer's catalog data, simplifies the complex thermodynamics processes in the AC compressor, condenser, expansion valve, and evaporator, properly reproducing the thermo-electrical performance of the AC. The dynamic performance of this model is validated here against the detailed model from [35], which has a total of 29 differential and

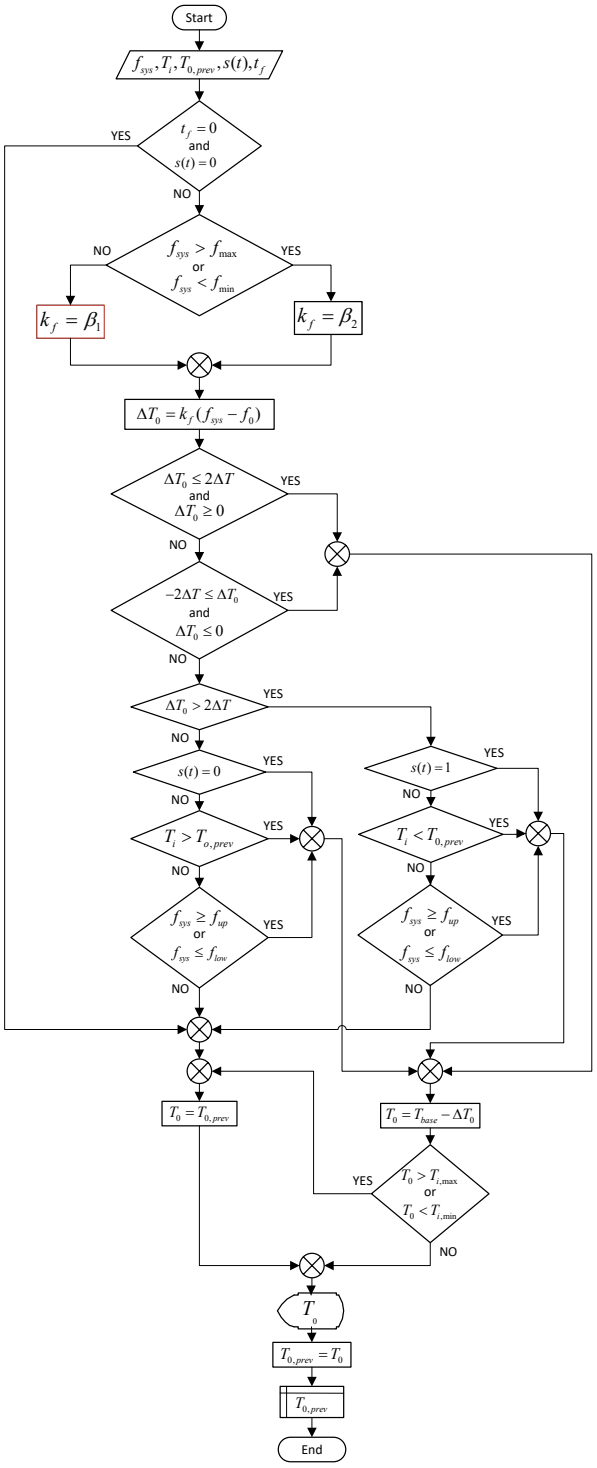


Fig. 13. Proposed DLC logic for ACs and GSHPs.

algebraic mass and energy conservation equations for seven different control volumes to reproduce the transient AC response. Fig. 15 shows the 12-hour simulation results obtained for both the model used here and detailed model from [35], for the 1930 W AC unit considered throughout, demonstrating the effectiveness of the equation-fit simplified model to properly reproduce the AC behavior (the maximum idle power error is 4.87 %). Note that the detailed model presents a relatively

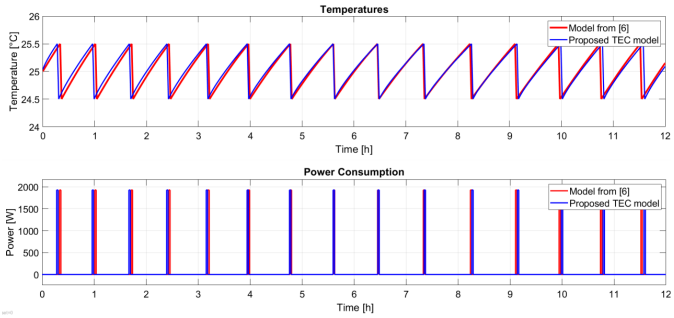


Fig. 14. Comparison between the proved model from [6] and the proposed household TEC model.

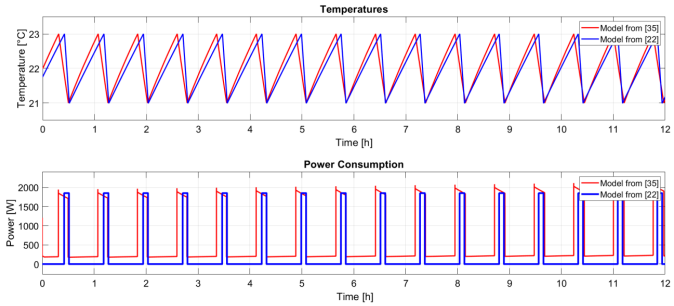


Fig. 15. Comparison between the detailed AC model from [35] and the adopted model.

small minimum power level associated with the power of compressor and fan in idle mode, which are not represented in the simplified model, but do not significantly affect the proposed ON/OFF frequency control strategy, since it is a small and constant power value.

C. GSHP

1) Household: The lumped parameter TEC model used to represent the household thermodynamic processes is the same as the one for the AC, which was previously validated.

2) Borehole: In order to capture the dynamics of the heat exchange between the borehole and its surrounding ground in a short-term basis, the TEC model developed in [26] is adopted here. This model has been validated in [36]–[39], and is able to accurately reproduce the dynamic behavior of the GHX under the ON/OFF transient operating conditions associated with the proposed frequency control approach, for both cooling and heating modes.

3) HP: As in the case of the AC, an equation-fit approach is used here to model the thermo-electrical behavior of the water-to-air HP through equations (9) and (10), which were adopted from [25]. The 6 coefficients of the 2 non-dimensional equations are determined by a least-square fit of the manufacturer's catalogue data, and is validated here for dynamic conditions against the equation-fit model in [22], which contains 4 equations and 22 coefficients, and whose performance has been validated against real data for several HPs. Fig. 16 depicts the 12-hour simulation results obtained for the HP model used in the simulation section versus the proven and more the detailed model from [22], with the

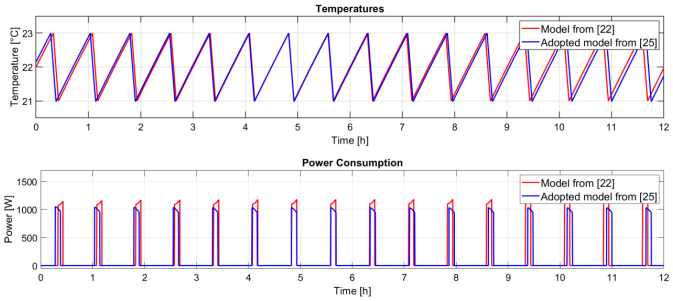


Fig. 16. Comparison between the proved GSHP model from [22] and the adopted model.

results showing a good agreement between both models (the maximum peak power error is 6.26 %), thus validating the simplified model used to represent the HP behavior in the context of the proposed ON/OFF frequency control approach.

D. Discussion

All of the aforementioned models were simulated using Matlab/Simulink (R2020a version) on a computer with an Intel(R) Core(TM) i7-8550U CPU @ 1.80GH processor. The simulations illustrated in Figs. 14, 15, and 16 for the household, AC, and water-to-air HP models, respectively, demonstrate the effectiveness of the models used here to capture the relevant thermo-electrical behavior by comparing their performance against existing proven models, since similar power levels and the same number of ON/OFF switching operations for the simplified and the detailed and validated models are obtained, thus allowing the use of the simplified models for the proposed frequency regulation approach.

In addition to their appropriate performance, the proposed models have low computational costs; thus, Table V shows the simulation times for 12 h in 1 s intervals for each model.Note that in the case of the household, the proposed TEC model is slightly higher due to the addition of a new differential equation to represent the heat transfer through the floor. For the AC, the adopted model, which only uses fit coefficients obtained from the manufacturer's catalog data off-line, is about 30 times faster than the detailed model, which requires solving many differential and algebraic equations, as well as thermal information about the status of the refrigerant across the AC's elements at each time step. Finally, for the GSHP, the calculation speed is about 2.2 times less for the simplified model used here, since their governing equations are simpler and require less information.

V. CASE STUDIES

In Canada, remote communities rely largely on diesel gensets with high costs for electricity generation ($ 0.13 to $ 2.45 per kWh [3]). In contrast, solar PV generation costs are up to $ 0.75 per kWh nowadays, and have been decreasing continuously [40]. Therefore, hybrid solar PV-diesel generation offers a promising cost-effective alternative for both reducing greenhouse emissions and lowering electricity costs in some regions, and thus such a system is studied next.

TABLE V
SIMULATION TIME COMPARISON

		Simulation time [s]
Household	Model from [6]	11.341
	Proposed TEC model	13.912
AC	Detailed model from [35]	345.74
	Adopted model from [22]	11.784
HP (GSHP)	Robust model from [22]	29.347
	Adopted model from [25]	13.247

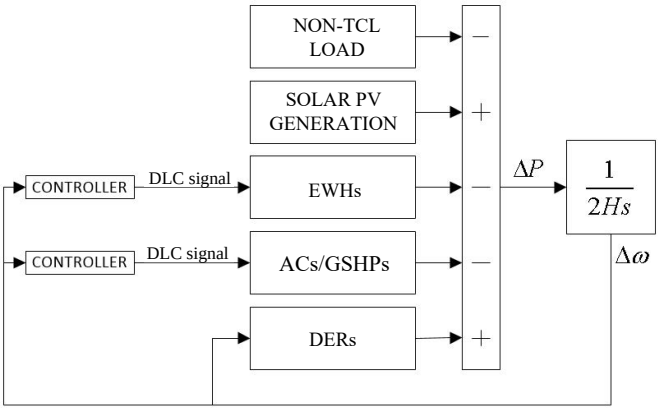


Fig. 17. Microgrid aggregated model for primary frequency regulation.

The microgrid of the Xeni Gwet'in First Nation community of British Columbia's remote Nemiah Valley, depicted in Fig. 18, has been extensively adopted as a test system for microgrid studies, since it was Canada's first battery-free PV-diesel off-grid network installed in 2007 [4], [8], [41], [42]. This microgrid is divided into two areas: (1) a commercial complex, and (2) a residential zone with 22 housing units. The generation plant houses three diesel gensets: two 95 kW gensets (operated one at a time), and a 30 kW genset that constantly operates within their efficient limits at weeknights and weekends. The characteristics of the 95 kW gensets are presented in Table VI.

A set of two 5.4 kW roof-top PV systems have been installed on each of the fourplexes, and there are two 2.88 kW roof-top PV systems on two different houses. The generation curve used to represent aggregated solar PV generation can be found in [16]. The load profile of the residential zone must represent the sudden and random demand variation among different households. Since this zone has 22 housing units, it is necessary to model individual load profiles to reflect realistic conditions. The number of occupants and the setpoint temperatures for ACs, GSHPs, and EWHs are randomly assigned. Then, by using the SRLS [6] and CREST [43] simulators, in addition to models presented in Section III, the load profile can be obtained [16]. The commercial load is adopted from [44], using it to create the daily load profile used here [16].

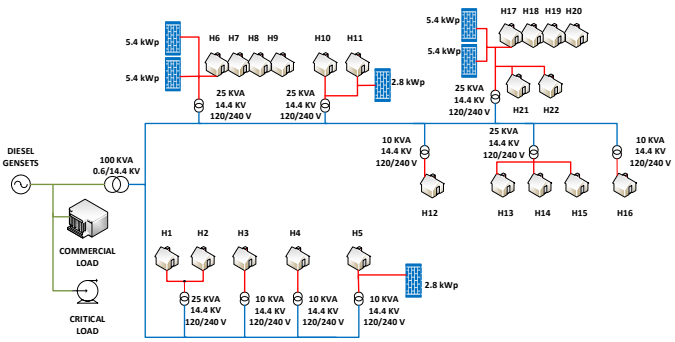


Fig. 18. Diagram of the Nemiah Valley's microgrid.

TABLE VI
CHARACTERISTICS OF THE 95 KW DEUTZ GENSET [41]

Engine BF69L13G	
Parameter	**Value**
P_G [kW]	95
V_T [V]	600
s_p [kW/Hz]	29.4
f_{nl} [Hz]	62.34

A. DR Control Logic

The parameters of the control logic are defined according to the characteristics of the Nemiah Valley's microgrid as presented in Table VII. The frequency limits are defined based on the operating range of the 95 kW genset, which corresponds to 30 to 90% of its available power. As this genset supplies power through a single-phase feeder, only 2/3 of the generator power is available; thus, the operating range of this generator is 28 to 64 kW. Hence, using its droop characteristic based on the data provided in TableVI, the frequency limits can be readily calculated to be $f_{lim,max}$ = 61.37 Hz and $f_{lim,min}$ = 60.33 Hz, which yields a central frequency of f_0 = 60.85 Hz in (21). These values are high compared to the standards defined by some utilities; however, the droop characteristic of the 95 kW diesel genset and the restriction imposed by the single-phase feeder yield such high values for this particular system, as also observed in [4], [8] and [42].

If f_{sys} exceeds the frequency limits, k_f increases by 10%. A delay t_D = 5 min in the initial activation and final deactivation of the DLC control among the TCLs' controllers is used to complement the control logic. Also, it is assumed that three households (about 14%) do not participate in frequency control. It should be mentioned that, in a typical weekday, the day's peak load is 75 kW with an average load of 29 kW without considering PV generation, which could be up to 27.36 kW. Therefore, the load variation plus the intermittent PV generation yield significant disturbances on the system frequency, making it challenging to efficiently operate these gensets on weekdays [41].

B. Case Studies and Simulation Results

The performance of the thermo-electrical models of TCLs along with the proposed DR strategy for primary frequency control are evaluated during the working hours of the 95 kW diesel gensets (6:30 a.m. to 11:30 p.m. on weekdays [41]), based on the following case studies:

C1. No control: In this case, only the diesel genset is responsible for balancing the demand plus the aggregated PV generation.
C2. EWHs' control: This study case illustrates the conventional control logic for EWHs presented in [8].
C3. Proposed EWHs' control: In this case, the proposed EWH control logic depicted in Fig. 12 is used.
C4. Proposed EWHs + ACs' control: The frequency control presented in C3 is complemented in this case by the control logic for ACs.
C5. Proposed EWHs + GSHPs' control: In this case, the performance of GSHPs replacing ACs for primary frequency control is evaluated, with the primary frequency control being shared among EWHs and GSHPs.

TABLE VII
PARAMETERES OF THE PROPOSED DR STRATEGY

Parameter	**EWHs**	**ACs/GSHPs**
T_{max} [°C]	60	25
T_{min} [°C]	49	23
T_{base} [°C]	54.5	24
k_f	10.37	10.86
f_{max} [Hz]	61.37	61.37
f_{min} [Hz]	60.33	60.33
f_0 [Hz]	60.85	60.85
f_{up} [Hz]	61.25	61.25
f_{low} [Hz]	60.47	60.47

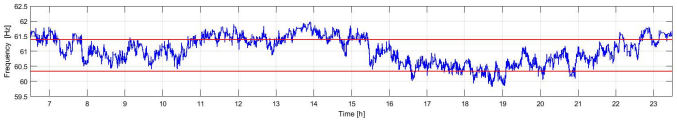
Fig. 19 depicts the system frequency response for all case studies considering identical thermal and electrical demand conditions. Note that the performance of the frequency control of the proposed EWH DR strategy (C3) improves compared to that in [8] (C2). In addition, as more TCLs, i.e., ACs (C4) or GSHPs (C5), are used to provide frequency control, the overall system response is better. The active power generated by the 95 kW diesel genset is depicted in Fig. 20 for the different study cases. Observe that as frequency control is added from the demand side, by means of the TCLs, the steep ramps are reduced significantly, thus helping the genset to respond more smoothly and very close, or within, its efficient operating limits.

Fig. 21 depicts the EWHs' temperatures for C1, C2, and C3, considering that three households do not participate in frequency control, as explained in Section V-A. In the first case, with no EWH control, each individual customer selects a setpoint temperature within the $T_{EWH,min}$ = 49°C and $T_{EWH,max}$ = 60°C safety range, resulting in the multiple temperature variations illustrated in Fig. 21(a). For C2 depicted in Fig. 21(b), and C3 shown in Fig. 21(c) the setpoints constantly vary over the operating time as EWHs are turned ON/OFF to provide frequency control; however, for C3, the temperatures are closer to each other, due to the controlled EWHs being tuned ON/OFF more often, thus resulting in better system frequency regulation.

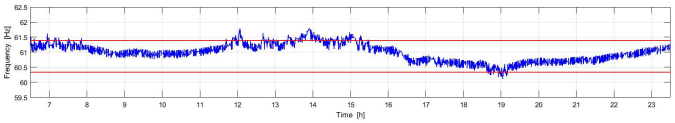
Fig. 22 illustrates the indoor temperatures for all households. Since the DR strategy for ACs and GSHPs is the

TABLE VIII
SIMULATION RESULT COMPARISON

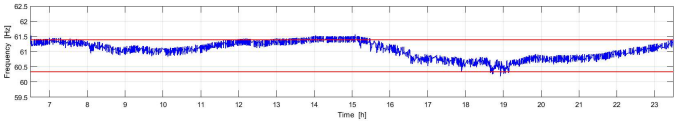
*		C1	C2	C3	C4	C5
Frequency *	f_{max} [Hz]	61.98	61.77	61.57	61.62	61.57
	f_{min} [Hz]	59.83	60.04	60.2	60.33	60.35
	σ [Hz]	0.4459	0.2969	0.2547	0.2507	0.2443
Power *	P_{max} [kW]	72.77	64.08	60.61	59.45	58.79
	P_{min} [kW]	11.61	16.72	25.5	25.01	23.97
Energy *	EWHs [kWh]	174.8	184.4	175.3	177.6	178.8
	ACs [kWh]	28.91	28.7	28.7	27.88	-
	GSHPs [kWh]	-	-	-	-	18.06
Fuel consumption [l]		207	210.8	205	205.2	203.6
Time f_{sys} exceeds limits [%]		32.22	10.58	7.55	4.16	7.15



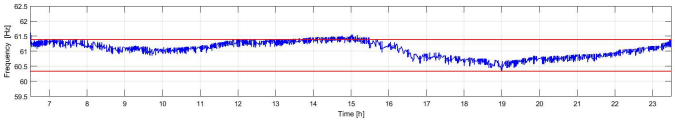
(a) Cl: No control.



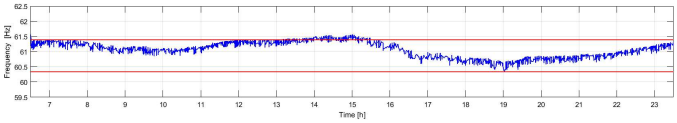
(b) C2: EWHs' control [8].



(c) C3: Proposed EWHs' control.

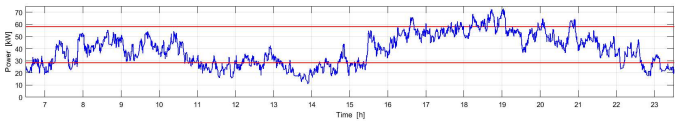


(d) C4: Proposed EWHs+ACs' control.

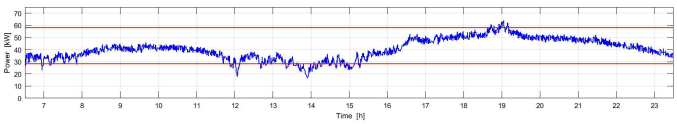


(e) C5: Proposed EWHs+GSHPs' control.

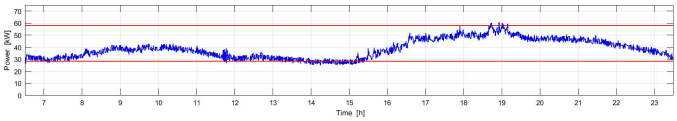
Fig. 19. System frequency response.



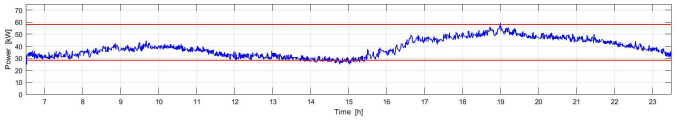
(a) Cl: No control.



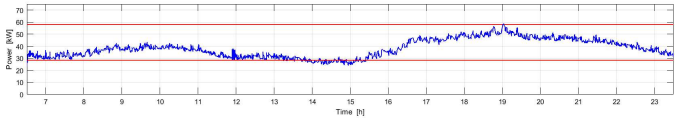
(b) C2: EWHs' control [8].



(c) C3: Proposed EWHs' control.



(d) C4: Proposed EWHs+ACs' control.

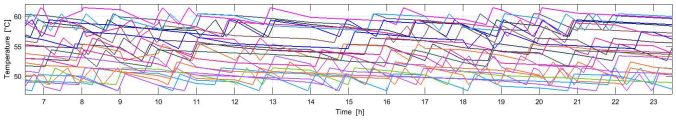


(e) C5: Proposed EWHs+GSHPs' control.

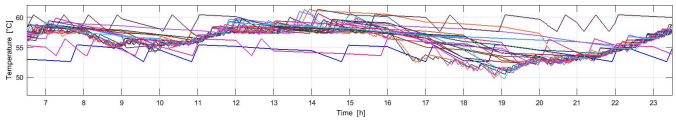
Fig. 20. Diesel genset active power.

same, only two cases are presented. Thus, in C1 illustrated in Fig. 22(a), the customers select their setpoints and no control is activated, whereas for C4 shown in Fig. 22(b), the setpoints vary over time. Since the safety range is narrow and considering that both ACs and GSHPs are compressor-based loads restricted by a lockout time after being turned OFF, observe that the setpoint adjustment is smother than that of EWHs.

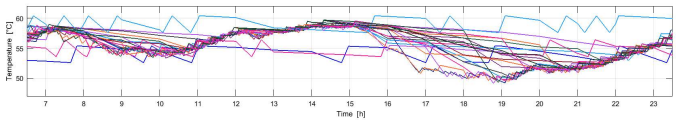
A summary of the simulation results of the five case studies is shown in Table VIII, presenting various performance parameters to evaluate the effectiveness of the proposed DR strategy for primary frequency control. Thus, observe that a DR strategy significantly improves the system performance irrespective of the TCLs used. For DR with EWHs in C2 and C3, the proposed strategy shows a better performance than that of [8], since the frequency variation range is narrower, and the energy consumed by the EWHs over the operating period, as well as the fuel consumption, are smaller. By including ACs and GSHPs in C4 and C5, the overall system performance improves, as these TCLs increase the demand flexibility for primary frequency control. The results in Table VIII show that the time the genset operates beyond its efficient limits is significantly reduced. Finally, note that GSHPs consume less energy than ACs, due to their energy storage capability.



(a) Cl: No control.

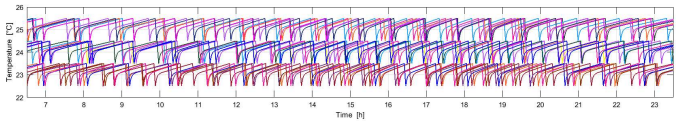


(b) C2: EWHs' control [8].

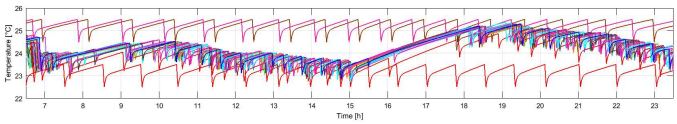


(c) C3: Proposed EWHs' control.

Fig. 21. EWHs' temperatures for all households.



(a) Cl: No control.



(b) C4: Proposed EWHs+ACs' control.

Fig. 22. Households' indoor temperatures.

VI. Conclusions

Thermo-electrical models of EWHs, ACs, and GSHPs have been proposed, capturing the relevant thermodynamic phenomena at reasonable computational costs, which allows to use them in DR dynamic studies. A novel DR strategy for frequency control has also been proposed, which based on the developed TCL dynamic models, was validated using a real microgrid. The results demonstrate the potential to provide primary frequency control with a TCL-based DR approach, thus facilitating a higher penetration of RES. It is important to mention that the paper demonstrates, with the help of a realistic microgrid example, that the implementation of the proposed DR control strategy for TCLs has significant potential to provide frequency regulation services, which is a main concern in isolated microgrids. Thus, the presented results could be used as a base to study and develop compensation strategies to attract customer participation in frequency control through TCLs for proper microgrid operation.

References

[1] M. Arriaga, C. A. Cañizares, and M. Kazerani, "Renewable energy alternatives for remote communities in northern Ontario, Canada," *IEEE Transactions on Sustainable Energy*, vol. 4, no. 3, pp. 661–670, July 2013.

[2] G. Papaioannou, I. Talavera, and J. Hanson, "The influence of diesel generators on frequency stability for isolated grids with high wind power penetration," *International Conference on Renewable Energies and Power Quality (ICREPQ'15)*, vol. 1, no. 13, pp. 616–621, March 2015.

[3] M. Arriaga, C. A. Cañizares, and M. Kazerani, "Northern lights: Access to electricity in Canada's northern and remote communities," *IEEE Power and Energy Magazine*, vol. 12, no. 4, pp. 50–59, July 2014.

[4] F. Katiraei, D. Turcotte, A. Swingler, and J. Ayoub, "Modeling and dynamic analysis of a medium penetration PV-Diesel Mini-Grid system," *4th European Conference on PV-Hybrid and Mini-Grid*, May 2008.

[5] P. J. Douglass, R. Garcia-Valle, P. Nyeng, J. Østergaard, and M. Togeby, "Smart demand for frequency regulation: Experimental results," *IEEE Transactions on Smart Grid*, vol. 4, no. 3, pp. 1713–1720, Sep. 2013.

[6] J. M. G. Lopez, E. Pouresmaeil, C. A. Cañizares, K. Bhattacharya, A. Mosaddegh, and B. V. Solanki, "Smart residential load simulator for energy management in smart grids," *IEEE Transactions on Industrial Electronics*, vol. 66, no. 2, pp. 1443–1452, Feb 2019.

[7] Environmental Protection Agency, "Geothermal heating and cooling technologies," Tech. Rep., 2017, [Accessed on 2019-08-15]. [Online]. Available: https://www.nrcan.gc.ca/energy/publications/efficiency/heating-heat-pump/6833

[8] K. Elamari and L. A. C. Lopes, "Frequency based control of electric water heaters in small pv-diesel hybrid mini-grids," in *2012 25th IEEE Canadian Conference on Electrical and Computer Engineering (CCECE)*, April 2012, pp. 1–4.

[9] A. Molina-Garcia, F. Bouffard, and D. S. Kirschen, "Decentralized demand-side contribution to primary frequency control," *IEEE Transactions on Power Systems*, vol. 26, no. 1, pp. 411–419, Feb 2011.

[10] P. J. Douglass, R. Garcia-Valle, P. Nyeng, J. Stergaard, and M. Togeby, "Smart demand for frequency regulation: Experimental results," *IEEE Transactions on Smart Grid*, vol. 4, no. 3, pp. 1713–1720, Sep. 2013.

[11] J. A. Short, D. G. Infield, and L. L. Freris, "Stabilization of grid frequency through dynamic demand control," *IEEE Transactions on Power Systems*, vol. 22, no. 3, pp. 1284–1293, Aug 2007.

[12] Z. Xu, J. Ostergaard, and M. Togeby, "Demand as frequency controlled reserve," *IEEE Transactions on Power Systems*, vol. 26, no. 3, pp. 1062–1071, Aug 2011.

[13] N. Lu and J. Hammerstrom, "Design considerations for frequency responsive grid friendly appliances," in *2005/2006 IEEE/PES Transmission and Distribution Conference and Exhibition*, May 2006, pp. 647–652.

[14] M. Gouda, S. Danaher, and C. Underwood, "Building thermal model reduction using nonlinear constrained optimization," *Building and Environment*, vol. 37, no. 12, pp. 1255 – 1265, 2002.

[15] M. Kummert and M. Bernier, "Sub-hourly simulation of residential ground coupled heat pump systems," *Building Services Engineering Research and Technology*, vol. 29, no. 1, pp. 27–44, 2008.

[16] W. Mendieta, "Thermostatically controllable loads for primary frequency control in isolated microgrids," Master's thesis, University of Waterloo, Canada, 2019.

[17] *2007 ASHRAE Handbook - Heating, Ventilating, and Air-Conditioning Applications (I-P Edition)*. American Society of Heating, Refrigerating and Air-Conditioning Engineers, Inc. (ASHRAE), 2007.

[18] S. Kavanaugh and K. Rafferty, *Ground-Source Heat Pumps: Design of Ground Source Heat Pump Systems*. American Society of Heating, Refrigerating and Air-Conditioning Engineers, Inc. (ASHRAE), 2014.

[19] C. Lin, C. Wu, J. Yang, and C. Liao, "Parameters identification of reduced governor system model for diesel-engine generator by using hybrid particle swarm optimisation," *IET Electric Power Applications*, no. 9, pp. 1265–1271, 2018.

[20] E. Nasr-Azadani, C. Canizares, and K. Bhattacharya, "Modeling and stability analysis of distributed generation," in *2012 IEEE Power and Energy Society General Meeting*, July 2012, pp. 1–8.

[21] U.S Department of Energy, "DHW event schedule generator," Tech. Rep. [Online]. Available: https://www.energy.gov/eere/buildings/building-america-analysis-spreadsheets

[22] C. Tang, "Modeling packaged heat pumps in a quasy-steady state energy simulator program," Master's thesis, Oklahoma State University, U.S., 2003. [Online]. Available: https://shareok.org/bitstream/handle/11244/10075/Tang_okstate_0664M_1318.pdf?sequence=1&isAllowed=y

[23] R. Stull, "Wet-bulb temperature from relative humidity and air temperature," *Journal of Applied Meteorology and Climatology*, vol. 50, no. 11, pp. 2267–2269, 2011. [Online]. Available: https://doi.org/10.1175/JAMC-D-11-0143.1

[24] TRANE, "Split system cooling product and performance data," Tech. Rep., 2019, [Accessed on 2019-08-10]. [Online]. Available: https://www.trane.com/commercial/uploads/pdf/1111/2ttb3.pdf
[25] A. Shenoy, "Simulation, modeling and analysis of a water to air heat pump," Master's thesis, Oklahoma State University, U.S., 2004. [Online]. Available: https://shareok.org/bitstream/handle/11244/10061/Shenoy_okstate_0664M_1183.pdf?sequence=1
[26] M. D. Rosa, F. Ruiz-Calvo, J. M. Corberán, C. Montagud, and L. A. Tagliafico, "A novel TRNSYS type for short-term borehole heat exchanger simulation: B2G model," *Energy Conversion and Management*, vol. 100, pp. 347–357, 2015.
[27] BOSH, "Residential Geothermal Heat Pumps," Tech. Rep., 2018, [Accessed on 2019-08-10]. [Online]. Available: https://www.bosch-climate.us/files/Greensource_BP_engineering_submittal_sheet_11.2018_US.pdf
[28] Q. Shi, F. Li, Q. Hu, and Z. Wang, "Dynamic demand control for system frequency regulation: Concept review, algorithm comparison, and future vision," *Electric Power Systems Research*, vol. 154, pp. 75 – 87, 2018.
[29] M. Farrokhabadi, C. A. Cañizares, and K. Bhattacharya, "Frequency control in isolated/islanded microgrids through voltage regulation," *IEEE Transactions on Smart Grid*, vol. 8, no. 3, pp. 1185–1194, May 2017.
[30] R. Diao, S. Lu, M. Elizondo, E. Mayhorn, Y. Zhang, and N. Samaan, "Electric water heater modeling and control strategies for demand response," in *2012 IEEE Power and Energy Society General Meeting*, July 2012, pp. 1–8.
[31] A. Kerim Kar and Ümit Kar, "Optimum design and selection of residential storage-type electric water heaters for energy conservation," *Energy Conversion and Management*, vol. 37, no. 9, pp. 1445–1452, Sep. 1996.
[32] M. H. Nehrir, R. Jia, D. A. Pierre, and D. J. Hammerstrom, "Power management of aggregate electric water heater loads by voltage control," in *2007 IEEE Power Engineering Society General Meeting*, 2007, pp. 1–6.
[33] V. Harish and A. Kumar, "Modeling and simulation of a simple building energy system," in *2016 International Conference on Microelectronics, Computing and Communications (MicroCom)*, 2016, pp. 1–6.
[34] A. Parvaresh, S. Mohammad, A. Mohammadi, and A. Parvaresh, "A new mathematical dynamic model for HVAC system components based on Matlab/Simulink," *International Journal of Innovative Technology and Exploring Engineering Energy and Buildings*, vol. 1, no. 4, 2012.
[35] J. Vargas and J. Parise, "Simulation in transient regime of a heat pump with closed-loop and on-off control," *International Journal of Refrigeration*, vol. 18, no. 4, pp. 235 – 243, 1995.
[36] M. De Rosa, F. Ruiz-Calvo, J. M. Corberán, C. Montagud, and L. A. Tagliafico, "Borehole modelling: a comparison between a steady-state model and a novel dynamic model in a real ON/OFF GSHP operation," *Journal of Physics: Conference Series*, vol. 547, Nov. 2014, 012008.
[37] F. Ruiz-Calvo, M. D. Rosa, J. Acuña, J. Corberán, and C. Montagud, "Experimental validation of a short-term Borehole-to-Ground (B2G) dynamic model," *Applied Energy*, vol. 140, pp. 210 – 223, 2015.
[38] A. Cazorla-Marin, C. Montagud, A. Montero, J. Martos, and J. Corberan, "Influence of different ground thermal properties in a borehole heat exchanger's performance using the B2G dynamic model," in *Proceedings of the IGSHPA Technical/Research Conference and Expo 2017*, 2017.
[39] I. Maestre, F. Gallero, P. Gómez, and J. Blázquez, "Experimental validation of a hybrid model for vertical ground heat exchangers under on-off operation conditions," *Energy and Buildings*, vol. 204, 2019, 109517.
[40] J. Royer, "Status of remote/off-grid communities in Canada," August 2011. [Online]. Available: http://publications.gc.ca/collections/collection_2013/rncan-nrcan/M154-71-2013-eng.pdf
[41] S. Pelland, D. Turcotte, G. Colgate, and A. Swingler, "Nemiah Valley photovoltaic-diesel mini-grid: system performance and fuel saving based on one year of monitored data," *IEEE Transactions on Sustainable Energy*, vol. 3, no. 1, pp. 167–175, Jan 2012.
[42] R. Tonkoski, L. A. C. Lopes, and D. Turcotte, "Active power curtailment of PV inverters in diesel hybrid mini-grids," in *2009 IEEE Electrical Power Energy Conference (EPEC)*, Oct 2009, pp. 1–6.
[43] R. Ian and T. Murray, "CREST domestic electricity demand model," Tech. Rep. [Online]. Available: https://dspace.lboro.ac.uk/dspace-jspui/handle/2134/5786
[44] D. Zhang, S. Li, P. Zeng, and C. Zang, "Optimal microgrid control and power-flow study with different bidding policies by using powerworld simulator," *IEEE Transactions on Sustainable Energy*, vol. 5, no. 1, pp. 282–292, Jan 2014.



William Mendieta received a diploma in Electrical Engineering from the University of Cuenca (Ecuador) in 2013 and completed his MASc in Electrical and Computer Engineering at the University of Waterloo (Canada) in 2019. He is currently pursuing the Ph.D. degree in the School of Electrical & Electronic Engineering at University College Dublin. He has previously worked as a protection and control engineer for generation, transmission, and distribution system networks. His research interests include modeling, analysis, and control of power systems.



Claudio A. Cañizares (S'85,M'91,SM'00,F'07) is a University Professor and Hydro One Endowed Chair at the ECE Department of the University of Waterloo, where he has been since 1993. His highly cited research focuses on modeling, simulation, computation, stability, control, and optimization of power and energy systems. He is the IEEE Trans. Smart Gird EIC; a Fellow of the IEEE, the Royal Society of Canada, and the Canadian Academy of Engineering; and is the recipient of the 2017 IEEE PES Outstanding Power Engineering Educator Award, the 2016 IEEE Canada Electric Power Medal, and of multiple awards and recognitions from PES Technical Committees.